Anharmonic properties in Mg_2X (X = C, Si, Ge, Sn, Pb) from first-principles calculations

Aleksandr Chernatynskiy* and Simon R. Phillpot
Department of Materials Science and Engineering, University of Florida, Gainesville, Florida 32611 USA
(Received 10 April 2015; revised manuscript received 22 June 2015; published 7 August 2015)

Thermal conductivity reduction is one of the potential routes to improve the performance of thermoelectric materials. However, detailed understanding of the thermal transport of many promising materials is still missing. In this paper, we employ electronic-structure calculations at the level of density functional theory to elucidate thermal transport properties of the Mg_2X (X = C, Si, Ge, Sn, and Pb) family of compounds, which includes Mg_2Si, a material already identified as a potential thermoelectric. All these materials crystallize into the same antifluorite structure. Systematic trends in the anharmonic properties of these materials are presented and examined. Our calculations indicate that the reduction in the group velocity is the main driver of the thermal conductivity trend in these materials, as the phonon lifetimes in these compounds are very similar. We also examine the limits of the applicability of perturbation theory to study the effect of point defects on thermal transport and find that it is in good agreement with experiment in a wide range of scattering parameter values. The thermal conductivity of the recently synthesized Mg_2C is computed and predicted to be 34 W/mK at 300 °C.

DOI: 10.1103/PhysRevB.92.064303 PACS number(s): 44.10.+i, 63.20.dk, 63.20.kg

I. INTRODUCTION

The Mg_2X materials, where X = C, Si, Ge, Sn, and Pb, are a family of II-IV compounds that are isostructural to each other in their most stable antifluorite phase. While the last four materials in the series have being known for a long time and have been extensively studied [1–6], Mg_2C has only recently been synthesized, under high pressure conditions [7]. Mg_2Si has recently attracted renewed interest due to remarkable thermoelectric properties for high temperature applications, especially in solid solution with Mg_2Sn. In particular, the figure of merit of $Mg_2Si_xSn_{1-x}$ reaches $ZT = 1.1$ at 800 K [8]. This material has other potential applications, such as near-infrared optoelectronics [9]. Mg_2Ge and Mg_2Sn can form a solid solution with each other and with Mg_2Si, thus allowing systematic modification of their properties. For example, the impressive thermoelectric performance of $Mg_2Si_xSn_{1-x}$ is associated with a decrease in the thermal conductivity associated with alloying. It is thus not surprising that a number of first-principles investigations of structural, thermodynamic, and electronic properties have been performed [5,6,10–13] recently, with results being in good agreement with available experimental data.

Thermal conductivity is an important factor in determining thermoelectric performance, yet the thermal transport properties from first principles are only available for Mg_2Si and Mg_2Sn [13,14]. While a recent investigation of Mg_2Si and Mg_2Ge determined phonon properties using a state-of-the-art approach (the quasiharmonic approximation using fully first-principles descriptions of the interatomic interactions), it used a traditional and approximate approach (the Slack formula) to obtain the thermal conductivity itself [11]. While such an approach results in reasonable agreement with experiment, it does not yield significant mechanistic insight into the thermal transport properties, such as the relative importance of the contributions of different phonon modes. Moreover, this method explicitly ignores contributions to the thermal transport from optical phonon modes; it is not a priori clear that they can be ignored. Indeed, the importance of optical modes was recently demonstrated experimentally and theoretically for fluorite-structured UO_2 [15] and theoretically for ionic compounds, such as MgO and $SrTiO_3$ [16]. At the same time, the complete series of Mg_2X compounds represents an interesting case for a comparative study of the thermal transport properties, due to the fact that the mass of one of the constituents varies, while the interatomic interactions remain similar because the X elements are isoelectronic to each other.

In this paper, we present calculations of the thermal conductivity of the Mg_2X series based on density functional theory (DFT) and the solution of the Boltzmann transport equation (BTE) for phonons. This approach has been used extensively over the last few years to produce quantitatively accurate results for the thermal conductivity of a number of materials [13–15,17–21]. We investigate the details of the thermal transport and demonstrate that optical modes are also important in this series of compounds. Further, we investigate the importance of isotopic disorder in these materials. Based on our calculations, strategies for the reduction of the thermal conductivity are suggested, which might further improve the thermoelectric properties of these compounds. The remainder of the paper is organized as follows: Section II introduces the computational methodology. Section III presents the main results of our paper and discussion; our conclusions are in Sec. IV.

II. COMPUTATIONAL METHODOLOGY

We compute thermal conductivity from first principles via the BTE approach encoded in the PhonTS software package developed by the authors [22] and described in detail elsewhere [23]. In short, the thermal conductivity is determined by computing the heat current using the nonequilibrium phonon density distribution function, which in turn is found as a solution of the linearized BTE for phonons. The BTE, in terms of the deviation $\Phi_{\vec{k},n}$ from the equilibrium distribution $f^0_{\vec{k},n}$ for phonons in state with wave vector $\vec{k}$ and branch n, takes the

*alextch@gmail.com

form

$$-\vec{v}_{\vec{k},n}\cdot\frac{\partial f^0_{\vec{k},n}}{\partial T}\nabla T=\frac{1}{k_BT}\left\{\sum_{\vec{k}',n';\vec{k}'',n''}\left[(\Phi_{\vec{k},n}+\Phi_{\vec{k}',n'}-\Phi_{\vec{k}'',n''})\Lambda^{\vec{k}'',n''}_{\vec{k},n;\vec{k}',n'}+\frac{1}{2}(\Phi_{\vec{k},n}-\Phi_{\vec{k}',n'}-\Phi_{\vec{k}'',n''})\Lambda^{\vec{k}',n';\vec{k}'',n''}_{\vec{k},n}\right]+\ldots\right\},\quad(1)$$

where $\vec{v}_{\vec{k},n}$ is the group velocity of the phonon; T is the temperature; k_B is the Boltzmann constant; Λ is the equilibrium transition rate for possible phonon-phonon interaction process. The left-hand side of Eq. (1) describes the drift of phonon into and out of a given volume element, while the right-hand side is responsible for the phonon-phonon interactions. The two key approximations employed in Eq. (1) are (i) the system is subject only to small deviations from equilibrium, which allow linearization in terms of the deviation $\Phi_{\vec{k},n}$ of the phonon distribution from the equilibrium distribution; and (ii) all small regions of the system are at local equilibrium, allowing the distribution function on the left-hand side to be treated as a function of temperature only, with the spatial dependence controlled via the temperature field and the treatment of the phonon-phonon interactions as a perturbation to the harmonic solution. In this approximation, only cubic anharmonicity is considered; that is 3-phonon processes are described, but processes involving four or more phonons are not included. This assumption is generally accurate at moderate temperatures studied here [24]. Perturbation theory provides expressions for the equilibrium transitions rates

$$\begin{aligned}\Lambda^{\vec{k}'';n''}_{\vec{k};n\vec{k}';n'}&=\frac{2\pi}{\hbar}\Gamma^2_{nn'n'';\vec{k}\vec{k}'\vec{k}''}f^0_{\vec{k};n}f^0_{\vec{k}';n'}\left(f^0_{-\vec{k}'';n''}+1\right)\delta(\hbar\omega_{\vec{k};n}+\hbar\omega_{\vec{k}';n'}-\hbar\omega_{-\vec{k}'';n''}),\\ \Lambda^{\vec{k}'';n''\vec{k}';n'}_{\vec{k};n}&=\frac{2\pi}{\hbar}\Gamma^2_{nn'n'';\vec{k}\vec{k}'\vec{k}''}f^0_{\vec{k};n}\left(f^0_{-\vec{k}';n'}+1\right)\left(f^0_{-\vec{k}'';n''}+1\right)\delta(\hbar\omega_{\vec{k};n}-\hbar\omega_{-\vec{k}';n'}-\hbar\omega_{-\vec{k}'';n''}),\\ \Gamma_{nn'n'';\vec{k}\vec{k}'\vec{k}''}&=i\frac{(\hbar/2)^{3/2}}{V^{1/2}}\omega^{-1/2}_{\vec{k};n}\omega^{-1/2}_{\vec{k}';n'}\omega^{-1/2}_{\vec{k}'';n''}\sum_{IJK}\frac{\bar{B}_{IJK;\vec{k}\vec{k}'\vec{k}''}}{m_I^{1/2}m_J^{1/2}m_K^{1/2}}\vec{e}^{\,*}_{I;\vec{k};n}\vec{e}^{\,*}_{J;\vec{k}';n'}\vec{e}^{\,*}_{K;\vec{k}'';n''},\end{aligned}\quad(2)$$

where $\hbar$ is Plank's constant, I, J, and K are indexes that count atoms of corresponding masses m in the primitive cell, V is the volume of the cell, while $\vec{e}_{I;\vec{k};n}$ is the eigenvector of the phonon with frequency $\omega_{\vec{k},n}$. Here, $\bar{B}_{IJK;\vec{k}\vec{k}'\vec{k}''}$ is a component of the Fourier transform of the cubic anharmonic energy term, while the δ functions enforce conservation of energy in the 3-phonon process. The required input for the BTE, therefore, are the second and third spatial derivatives of the total energy with respect to atomic positions, which we obtain from the DFT calculations described below. The solution of the BTE itself is found by the iterative technique, using the conventional cubic fluorite unit cell with a $9\times9\times9$ k-point mesh, except for Mg_2C, where convergent results require a denser $13\times13\times13$ mesh. Since the thermal conductivity of Mg_2X materials is fairly small (on the order of 10 W/mK) around room temperature, the results from iterative solution are only marginally different from those obtained with the relaxation time approximation [23].

Other anharmonic properties presented in this paper are computed using the following approaches. Thermal expansion is obtained via the quasiharmonic approximation [25,26], which produces the dependence of the volume on temperature. The linear thermal expansion coefficient is then calculated using the standard formula

$$\alpha=\frac{1}{L}\frac{\partial L}{\partial T}.\quad(3)$$

Grüneisen parameters $\gamma_{\vec{k};n}$ of the individual phonon modes by definition as

$$\gamma_{\vec{k};n}=-\frac{\partial\ln\omega_{\vec{k};n}}{\partial\ln V}.\quad(4)$$

These derivatives are computed numerically by varying the volume of the simulation cell. Averaged Grüneisen parameters reported here are simple averages over the Brillouin zone.

The second and third derivatives of the total energy that are required for the calculations above are obtained via numerical differentiation of the DFT forces due to finite displacements of the atomic positions. All DFT calculations are performed using the Vienna *Ab initio* Simulation Package (VASP) computational package [27–30]. In particular, we use the local-density approximation (LDA) and the generalized gradient approximation, Perdew-Burke-Ernzerhof (GGA-PBE) approximations for the exchange-correlation functional, together with the projector-augmented wave (PAW) [31,32] treatment of the core electrons. All calculations are performed using a $2\times2\times2$ supercell of 96 atoms and a $2\times2\times2$ k-mesh for the representation of the electronic Bloch wave function, which is expanded in a plane-wave basis with energy cutoff of 500 eV. We verified that denser k-point mesh ($4\times4\times4$) and larger real space cutoff ($3\times3\times3$ supercell) result in negligible differences for phonon frequencies. For Mg_2C, the mean square differences in phonon frequencies are 0.0012 and 0.075 THz, correspondingly. For Mg_2C, Mg_2Si, and Mg_2Ge, where DFT calculations predict a nonzero electronic gap, Born effective charges are computed via a separate calculation which employs density functional perturbation theory in a primitive cell with a $7\times7\times7$ k-point mesh. These Born effective charges are needed to properly account for the long-range electrostatic contribution to the phonon structure.

III. RESULTS AND DISCUSSION

The basic structural and elastic properties of the Mg_2X materials were outlined in recent publications [5,6,10]; thus, we do not present these results, other than noting that our calculations of the lattice constants are in close agreement with the reported values. The data presented in Table I lists lattice constant at 300 K obtained via the quasiharmonic approximation; thus, these lattice constants take into account

TABLE I. Basic properties of Mg_2X relevant for thermal transport properties.

	Mg_2C	Mg_2Si	Mg_2Ge	Mg_2Sn	Mg_2Pb
a (Å) at 300 K					
LDA	5.3953	6.2974	6.3349	6.7177	6.8218
PBE	5.4462	6.3954	6.4596	6.8562	6.9688
Experiment		6.2678 [35], 6.338–6.391 [36]	6.378 [37], 6.378–6.380 [36]	6.750–6.780 [36]	6.760–6.836 [36]
Thermal expansion ($\times 10^5$ K^{-1}, at 300 K)					
LDA	1.52	1.47	1.61	1.69	2.2
Experiment		1.09 [38], 1.0 [3], 1.23 [39]	1.46 [40], 1.4 [3], 1.5 [41], 1.46 [39]	1.0 [3]	
Speeds of sound (m s^{-1})					
Transverse, LDA	4622	4450	3450	2960	2290
Transverse, Exp.		4830–4970		~3000 [42]	
Longitudinal, LDA	10 617	7680	6040	5140	4000
Longitudinal, Exp.		7650–7680		~5000	
Debye temperature (K)					
Θ_D (K), LDA	660	534	412	334	254
Θ_D (K), Exp. [34]		578	492	340	275
Grüneisen parameter of the Raman active F_{2g} mode					
LDA	1.14	1.36	1.33	1.35	1.48
Experiment		1.13–1.36 [3]	1.10–1.45 [3]	0.9–1.34 [3]	
Average Grüneisen parameter					
LDA	1.57	1.40	1.41	1.34	1.60
Experiment		1.32 [43]	1.38 [43]	1.27 [43]	

thermal expansion and are slightly greater than the zero-temperature value presented by Pandit and Sanyal [5]. These results show the expected trends from using LDA and PBE density functionals: LDA predicts lattice constants about 1–2% smaller than PBE. Comparison with the experimental data, which also has some scatter, shows that that PBE consistently overestimates the lattice constant, while LDA underestimates, with LDA overall providing somewhat smaller error. The issue of having an accurate lattice constant is important due to the sensitivity of the thermal conductivity to the simulation volume [20] as we discuss in detail below. Therefore, we use the LDA density functional in the remainder of this paper.

Other phonon-related and anharmonic properties presented are the speed of sound, Debye temperature, coefficient of thermal expansion, and average Grüneisen parameters. All of these parameters agree rather well with the experimental data where available. The Debye temperature Θ presented here is computed on the basis of the longitudinal (v_L) and transverse (v_T) speeds of sound via the following standard formula [33]:

$$\Theta = \frac{h}{k_B}\left(\frac{3N}{4\pi V}\right)^{1/3}\left(\frac{1}{3v_L^3}+\frac{2}{3v_T^3}\right)^{1/3}, \qquad (5)$$

where N is the number of atoms in the cell and V is the volume. This is compared with the experimental estimates that are based on the elastic constants measurements [34] of the Debye temperature near 0 K. The speed of sound and Debye temperature show the same trend of decreasing with increasing mass of the X component. The coefficient of thermal expansion as determined from the quasiharmonic approximation shows the opposite trend: increasing with the increased mass of X. Since the thermal expansion is a basic anharmonic effect this trend might indicate increased anharmonicity with increasing X. Comparison with experimental data, where available, shows that the DFT-LDA tends to overestimate thermal expansion in this series of compounds. Finally, the Grüneisen parameter of the Raman active F_{2g} phonon mode, which is experimentally accessible, agrees with the upper range of the available experimental data [3] and steadily increases across the series, although it is very similar for the Si, Ge, and Sn compounds. The average Grüneisen parameter, on the other hand, does not show a definite trend, being very similar for Mg_2Si and Mg_2Ge, slightly smaller for Mg_2Sn and significantly larger for Mg_2Pb. Experimental values available in the literature show the same trend, but of slightly greater magnitude. Somewhat surprisingly, the Grüneisen parameter of Mg_2C is similar to that of Mg_2Pb.

From the fundamental perspective, the phonon structure of a material is controlled by two factors: the masses of the compounds and details of the interatomic interactions. In Mg_2X, the mass of one of the elements increases going down the series, while the interactions between atoms, though similar due to the same valence electron shell structure, nevertheless show some differences. The traditional picture invokes mixed ionic-metallic bonding, with metallicity steadily increasing down the periodic table [44]. Many experimental investigations of Mg_2Si [45,46] and the limited experiments on Mg_2Si, Mg_2Ge, and Mg_2Sn [47] assumed bonding as covalent-ionic and estimated effective charges and the degree of ionicity. Recent DFT calculations, however, clearly identify the metallic-ionic character of the bond, since the Born effective charge tensors are essentially diagonal [48], and there is no appreciable bond charge densities present in the electronic density distributions in these compounds [4,7,48]. From the electronic properties perspective, Mg_2C, Mg_2Si, Mg_2Ge, and Mg_2Sn are all indirect gap semiconductors with

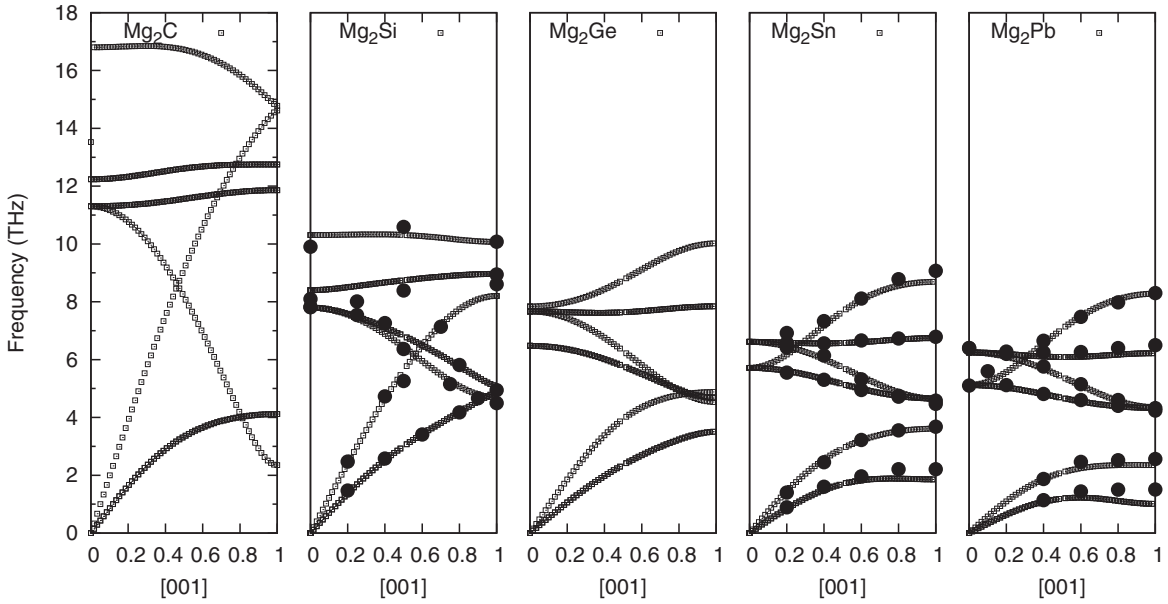

FIG. 1. Comparison between phonon dispersions in 001 direction of the Brillouin zone (BZ) by LDA calculations. Circles are experimental data from inelastic neutron scattering available for Mg_2Si [47], Mg_2Sn [48], and Mg_2Pb [49].

decreasing gaps for the latter three compounds of 0.77, 0.74, and 0.34 eV [49]. Our DFT calculations predict smaller gaps of 0.13, 0.17, and 0.0 eV, respectively, slightly smaller than the DFT-GGA data of 0.23, 0.17, and 0.0 eV reported previously [12]. Our result for Mg_2C is 0.75 eV, slightly greater than the DFT-PBE result of 0.67 eV reported in the literature [7]. An underestimate of the band gap is a well-known deficiency of the LDA, even to the extent of vanishing gap in Mg_2Sn. While these smaller predicted gaps than the experimental values are unlikely to affect thermal conductivity calculations presented here, the vanishing gap in Mg_2Sn can be expected to lead to a slight error. This is due to the fact that Born effective charges cannot be defined for a zero-gap material, and thus electrostatic long-range contribution to the phonon band structure will be absent in the calculations for Mg_2Sn. In our previous investigation of thermal conductivity in ionic compounds [16], such an omission resulted in the error of about 10% in the fluoride-structured material. Finally, Mg_2Pb is a semimetal experimentally, as well as from the DFT calculations.

In Fig. 1, we present the phonon dispersion curves in Mg_2X along the Γ-X direction in the Brillouin zone. Where available, results of our calculations are compared with the inelastic neutron scattering data [50–52]. First, we note the very good agreement between measured and calculated phonon frequencies. Second, we observe longitudinal optical-transverse optical (LO-TO) splitting in Mg_2C, Mg_2Si, and Mg_2Ge, a result of nonzero effective charges predicted by LDA in these compounds. This splitting is directly proportional to the Born effective charges and is thus a measure of the accuracy of their determination. In Mg_2C, the LO-TO splitting is 4.6 THz, in excellent agreement with the previously calculated value of 4.8 THz [53]. The LO-TO splittings in Mg_2Si and Mg_2Ge are calculated to be 1.9 and 1.4 THz as compared with the corresponding experimental values of 1.8 and 0.9 THz [1,47]. This overestimation for Mg_2Ge was already noted in previous work [10]. In our LDA calculations, due to their zero energy gap and thus zero Born effective charges, neither Mg_2Sn nor Mg_2Pb displays a LO-TO splitting. Further, we note that the acoustic branches show the clear influence of the mass of X. In particular, the energy of the longitudinal acoustic (LA) mode at the X point decreases with increasing mass of X. This effect is not nearly as pronounced for the transverse mode, which covers a very similar range of energies in Mg_2C, Mg_2Si, and Mg_2Ge, but has lower energy at the X point for the two heaviest compounds in the series. The speeds of sound reported in Table I naturally reflect the same trend. Finally, the optical modes are not nearly as sensitive to the changes in the X compound as the acoustic modes, with the exception of the lightest compound in the series Mg_2C. The biggest difference is a somewhat lower maximum energy and the already mentioned lack of an LO-TO splitting in Mg_2Sn and Mg_2Pb, as compared to Mg_2Si and Mg_2Ge.

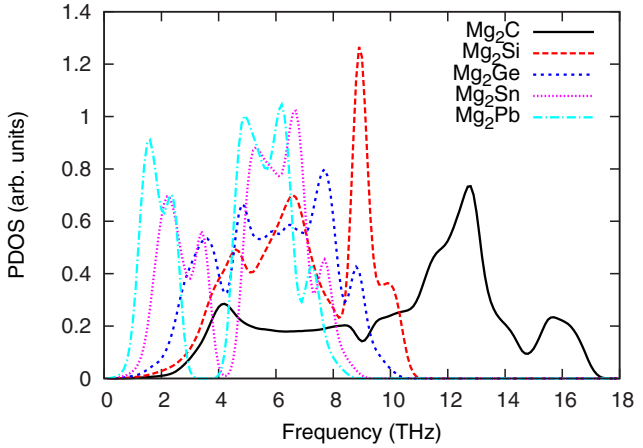

FIG. 2. (Color online) Comparison of phonon densities of states in Mg_2X (X = C, Si, Ge, Sn, and Pb) from DFT/LDA.

Figure 2 presents the phonon density of states (PDOS) as computed by DFT-LDA and smoothed with a Gaussian function with a width of 0.3 THz. The PDOS aggregates information about all phonons in the system, not only those from the specific high-symmetry directions in Fig. 1. The peaks of the PDOS curve correspond to the phonon energies at the Brillouin zone edges, since these occupy the largest volume in the reciprocal space. For example, the PDOS of Mg_2Pb features five peaks: at 1.7, 2.4, 5.0, 6.5, and 7.2 THz. These correspond to the TA, LA, TO_1, LO_1, and LO_2 mode energies at the boundary of the Brillouin zone, as can be seen by comparison with Fig. 1. Additionally, the absence of states between 3 and 4 THz indicates the presence of a phonon gap in Mg_2Pb, as well as a very small gap in Mg_2Sn around 4 THz. The PDOS has been recently measured by the inelastic neutron scattering (INS) for Mg_2Si [39,54], Mg_2Ge [39], and Mg_2Sn [54]. Our simulations agree well with these experimental data. In particular, in Mg_2Ge, the PDOS is characterized by four peaks with frequencies from our simulations of 3.6, 4.9, 7.7, and 8.9 THz, in excellent agreement with the experimental values of 3.6, 4.7, 7.7, and 8.8 from Bessas *et al.* [39]. This comparison is important since the data of Bessas and coworkers to our knowledge is the only available data on phonon properties from the inelastic neutron scattering, as opposed to Mg_2Si, Mg_2Sn and Mg_2Pb, where measurements of the full dispersions are available, as discussed earlier.

We now turn our discussion to the anharmonic properties of the Mg_2X series of compounds. In Fig. 3, we present the thermal expansion coefficient as computed in the quasiharmonic approximation as a function of temperature in the range of 0–800 K. Experimental data for the entire series is rather scarce, with the most complete data available for Mg_2Ge [3,40,41] and a single source for Mg_2Si and Mg_2Sn [3]. Our results slightly overpredict the thermal expansion for the Mg_2Ge, the compound with the most reliable and consistent experimental data, as was already noted in the discussion of Table I. While our results for Mg_2Si and Mg_2Sn overestimate experiment by about 50%, they are in the excellent agreement with the results of the previous DFT/GGA calculations [11]. The thermal expansion curves in Fig. 3 show standard behavior, with nearly constant expansion in the classical, high temperature regime and a decay to zero in the quantum regime

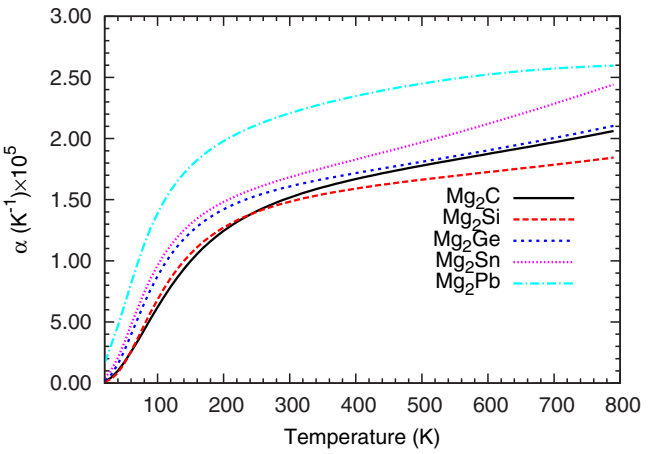

FIG. 3. (Color online) Thermal expansion of Mg_2X from DFT/LDA calculations in the quasiharmonic approximation.

at lower temperature. The first four compounds in the series all have comparable thermal expansions, with differences of no more than 10% among them below 500 K. Above this temperature, the thermal expansion of Mg_2Sn increases faster than those of the other compounds, with the increase in Mg_2Si being the slowest. The quasiharmonic approximation is intrinsically a low temperature analysis; thus, results at high temperature should be treated with caution. Mg_2Pb stands out among the entire series with thermal expansion predicted to be greater than that of other compounds by about 40% in the entire temperature range. Unfortunately, no experimental data is available to verify this prediction. In viewing thermal expansion as an anharmonicity measure, no systematic trends can be extracted from this data.

In Fig. 4(a), we present the results of the lattice thermal conductivity calculations for Mg_2X compounds in the temperature range of 100–800 K. For all compounds, the lattice thermal conductivity as a function of temperature is almost linear in this log-log plot, and thus is well described as a power law $k \sim T^{-\alpha}$. Using this power law and fitting to the data points above the Debye temperatures only in order to avoid quantum effects produces exponents very close to unity, as predicted by the Klemens theory [24]. In Fig. 4(b), we plot

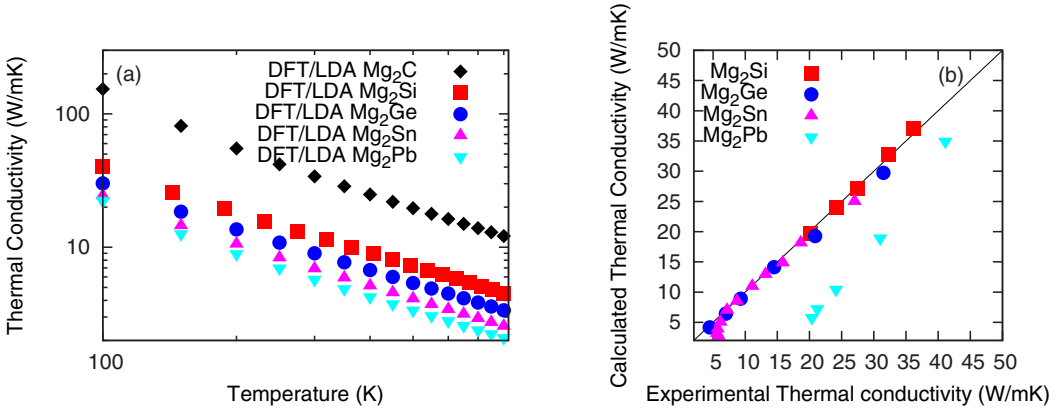

FIG. 4. (Color online) (a) Lattice thermal conductivities of Mg_2X, X = C, Si, Ge, Sn, Pb as computed by DFT/LDA with BTE shown in a log-log plot to demonstrate the power law dependence on temperature. (b) The same plotted versus available experimental data [2]; points on the diagonal signify good agreement with experiment.

the calculated thermal conductivities versus experimentally available ones; in this plot, the closer a given point is to the diagonal line, the better is the agreement with experiment. First, we note the excellent agreement with the experimental data available for Mg_2Si, Mg_2Ge, and Mg_2Sn. Our results for Mg_2Si and Mg_2Sn are also in excellent agreement with previous calculations by similar methods [13,14]. The greater values of experimentally measured thermal conductivity in Mg_2Sn for $\kappa < 7\,W/mK$ (those correspond to temperatures above $\sim$300 K) are due to the electronic contribution; thus, this is not captured by our phonon calculations. The last compound in the series Mg_2Pb is a semimetal, and in this compound, the electronic contribution is pronounced at all temperatures; thus, the experimental values are larger in the entire temperature range. We discuss the thermal transport in this material separately below.

As we have mentioned in the beginning of this section, DFT within LDA produces slightly smaller errors for the basic structural properties than DFT within GGA-PBE. We nevertheless assess the differences between these two approaches for the thermal conductivity calculations. Comparison for Mg_2Si and Mg_2Ge is shown in Fig. 5, together with the experimental data. It is clear that LDA shows excellent agreement, while PBE is inconsistent. It results in very close agreement for Mg_2Si, while producing values substantially lower than both LDA and experiment for Mg_2Ge. In the previous work by the authors on thermal transport in solid argon, such an underestimation was attributed to the volume effect [20], as PBE tends to produce larger equilibrium volume than LDA, which in turn results in softer phonon modes and lower thermal conductivity. While this is the case for Mg_2Ge, in Mg_2Si, only the two highest optical modes appear to be softer within PBE as compared with LDA calculations. As a result, thermal conductivity is almost the same within these two approaches for Mg_2Si. We conclude that LDA seems to be preferable for thermal conductivity calculations, since PBE in general is expected to slightly overestimate equilibrium volume and thus to be prone to underestimation of thermal conductivity.

Mg_2Pb is the only semimetal material in the Mg_2X family, and thus has contributions from both phonons and electrons at all temperatures. The thermal conductivity of Mg_2Pb was

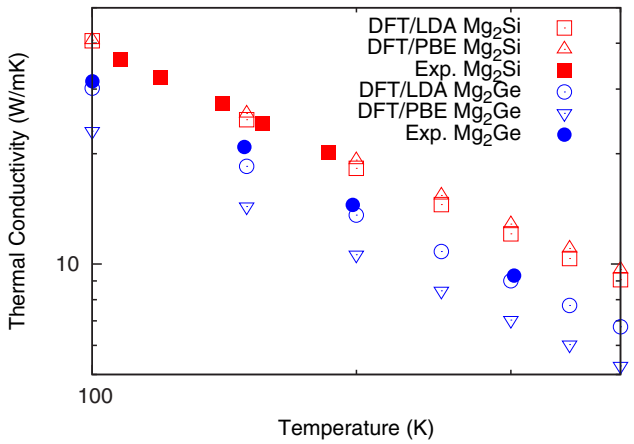

FIG. 5. (Color online) Comparison between LDA and PBE results for Mg_2Si and Mg_2Ge.

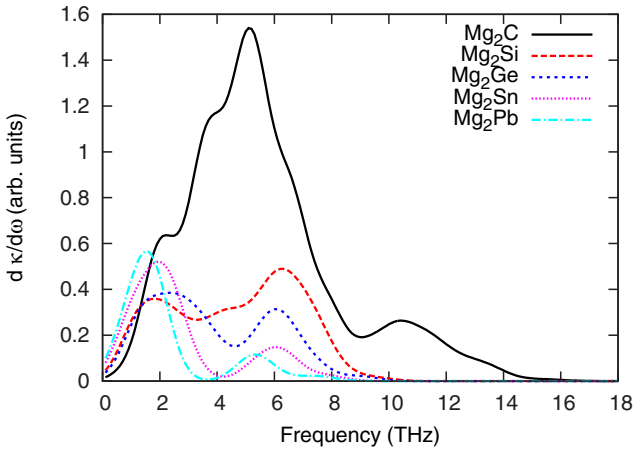

FIG. 6. (Color online) Spectral thermal conductivity as a function of phonon frequency in Mg_2X from LDA calculations.

carefully examined by Martin and Shanks [2] who measured overall thermal conductivity and electrical resistivity in order to differentiate different components. By estimating the electronic contribution on the basis of the Wiedemann-Franz law, they deduced that the lattice thermal conductivity of Mg_2Pb is larger than that of Mg_2Sn. In light of the significantly heavier mass of Pb in exactly the same structure, this situation was considered unlikely. A direct estimate of the phonon-mediated lattice component from the Leibfried and Schlomann equation [55] and data for Mg_2Sn concluded that the lattice thermal conductivity of Mg_2Pb is smaller than that of Mg_2Sn, as was indeed expected. To resolve this discrepancy, it was suggested that there is a significant bipolar contribution to the electronic thermal transport [56], similar to that in semiconductors at high temperature. Our calculations have direct access to Mg_2Pb lattice thermal conductivity and indeed show lower values than that of Mg_2Sn. This is consistent with the conclusion reached by Martin and Shanks that some other than pure electronic mechanism, such as bipolar contribution, can be significant in semimetals reaching $\sim$50% of the electronic thermal transport in Mg_2Pb in the 50–200 K temperature range.

To gain a deeper insight into the thermal transport properties of the Mg_2X series, we present spectral thermal conductivity data in Fig. 6 and individual phonon lifetimes in Fig. 7, both at 300 K. Spectral thermal conductivity is defined similarly to the PDOS

$$D^{\kappa}(\omega) = \frac{\partial \kappa(\omega)}{\partial \omega} = \sum_{\vec{k};n} \kappa_{\vec{k};n} \delta(\omega - \omega_{\vec{k};n}), \qquad (6)$$

where $\kappa_{\vec{k};n}$ is a contribution to the thermal conductivity from the mode with frequency $\omega_{\vec{k};n}$. We note that spectral thermal conductivity in Fig. 6 plotted with larger Gaussian widening (0.8 THz) of the individual states than the PDOS figures plotted in Fig. 2 due to the much coarser grids feasible for thermal conductivity calculations; they thus show fewer features. The common trait of all the curves is a double peak in the contributions to thermal conductivity, both of which gradually shift to lower frequencies. In Mg_2C, the first peak is produced by all the TA, LA, and LO modes, while the second peak is produced by the LA mode, since this is the only mode in

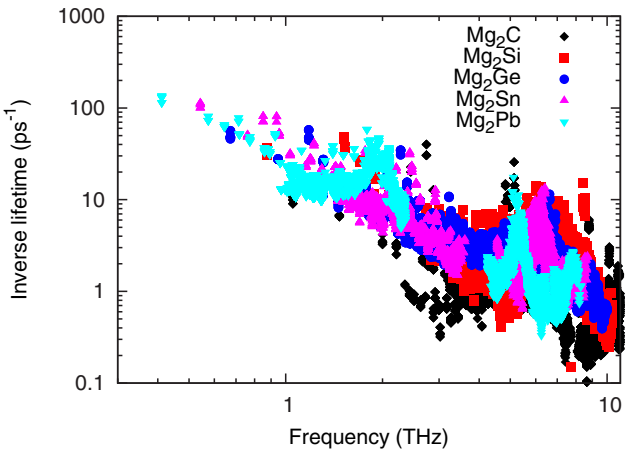

FIG. 7. (Color online) Phonon lifetimes as a function of frequency in Mg_2X.

this energy range with appreciable group velocity. In Mg_2Si, the LO mode can only contribute to the second peak, since the first peak is outside of its energy range; however, in this compound, the peaks overlap considerably. In the remaining compounds, the LO mode has very little or no overlap with the acoustic modes; thus, in Mg_2Ge, Mg_2Sn, and Mg_2Pb, the second peak arises exclusively from the optical modes, and their contribution progressively diminishes. According to our calculations, their contributions to total thermal conductivity are 35, 21, and 18%, respectively. The first peak, due to the acoustic modes, becomes progressively taller and narrower: this reflects the same trend in the PDOS shown in Fig. 2.

The individual phonon lifetimes, Fig. 7, show the general features that have being discussed in other materials [19,20]. Namely, the low frequency part of the spectrum can be fitted reasonably well with a second degree polynomial; however, at higher frequencies, the dependence is in fact nonmonotonic. A surprising feature, however, is the comparison between different materials: for the entire series of Mg_2X compounds, the phonon lifetime bands overlap with each other and do not show significant differences. This indicates that the decreasing trend in the thermal conductivity with increased mass of X in the Mg_2X series is dominated by reduction of the group velocity of the phonons, or speed of sound (see Table I). This conclusion generalizes a similar observation made from the limited study of Mg_2Si and Mg_2Sn materials [13].

Finally, we considered the degradation of the thermal conductivity by addition of the point defects in the Mg_2Si, the most promising of these materials for thermoelectric applications. The presence of the point defects introduces two distinct effects: mass disorder scattering and alteration of the local interatomic constants around the defect. For a low concentration of the defects, perturbation theory can be expected to apply: it adds an additional term in the BTE [17,57] linearly proportional to the scattering parameters Γ, which are a simple sum of contributions from mass and elastic disorder. The mass disorder term permits rigorous calculation [24], including the contribution from different sublattices [57]; however, the effect of altered interatomic interactions is much less well understood. Thus, we consider only the mass disorder term, which provides a lower bound of the reduction in the thermal conductivity (i.e., an upper bound to the thermal conductivity itself). The mass disorder term is a combination of the concentration of the defects and the mass difference between defect atoms and atoms of the host material and, when expressed in the form of the relaxation time associated with the defect scattering, is given by [57]

$$\tau^{-1}_{\vec{k};n} = \frac{\pi}{2N}\omega^2_{\vec{k};n}\sum_{\vec{k}';n'}\delta(\omega_{\vec{k};n}-\omega_{\vec{k}';n'})\sum_I g_I|\vec{e}^{\,*}_{I;\vec{k}',n'}\cdot\vec{e}^{\,*}_{I;\vec{k},n}|^2, \tag{7}$$

Here, g_I is the scattering parameter associated with atom I in the primitive cell, while all the other notations are the same as in Sec. II. Equation (7) is applicable at any concentration for defects of almost the same mass as the host, such as the case of isotopic substitutions, and only at small concentrations if the masses are substantially different. Scattering parameters are computed using the following expression [57]

$$g_I = \sum_i f_i^I\left(1-\frac{M_i^I}{\bar{M}^I}\right)^2, \tag{8}$$

where i counts possible isotopes/substitutions for atom I, f_i^I and M_i^I give concentration and mass of the ith impurity, while $\bar{M}^I$ is the average mass. In case of the Mg_2Si, most of the alloying elements of interest substitute into the Si sublattice; thus, it is interesting to illuminate the effect of varying scattering parameter for this sublattice. Correspondingly, the Mg sublattice experiences isotopic disorder only, and its scattering parameter is held constant. Results of the calculations of the variation of thermal conductivity with scattering parameter for Si sublattice are shown in Fig. 8, where the vertical lines denote the values for the scattering parameters for impurities of different masses and concentrations.

We observe that the limits of applicability of the perturbative treatment of the point defects have not being thoroughly explored in the literature. Isotopic defects are characterized by

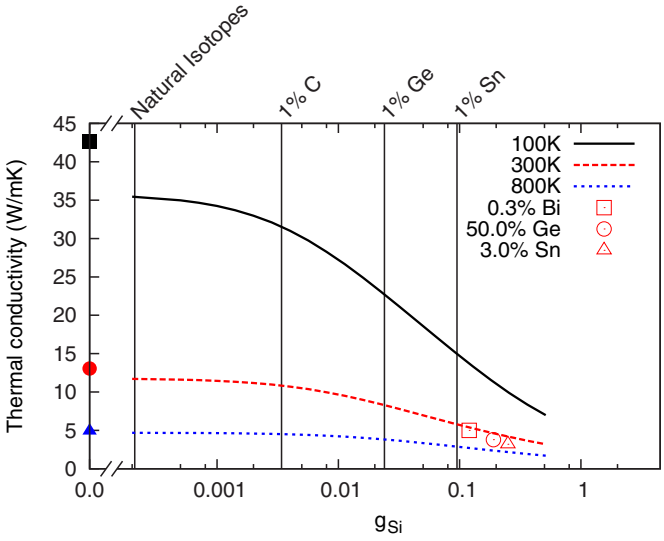

FIG. 8. (Color online) Thermal conductivity in doped Mg_2Si as predicted by perturbation theory at different temperatures. Data for Sn (virtual crystal approximation) [13], Bi [53], and Ge [54] (experimental) are at 300 K.

very small values of the scattering parameters, driven by the small change in the defects mass. In Mg_2Si, these values are found to be 0.00074 for Mg and 0.0002 for Si, as indicated in Fig. 8; in this regime, perturbation treatment can be expected to be reliable, as was explicitly demonstrated in the case of pure Si and Ge [17]. Reduction of thermal conductivity due to isotopic contribution in Mg_2Si at room temperature is about 10%, in excellent agreement with the work of Li *et al.* [13]. However, upon substitution with atoms of very different mass even at the modest concentrations of $\sim$1%, the value of the scattering parameter increases rapidly, as can be seen in Fig. 8 for the cases of C, Ge, and Sn substitutions at 1% into the Si sublattice. For instance, for a 1% substitution of Sn, the scattering parameter reaches the value of 0.095. In order to assess the applicability of the perturbation treatment in this regime, we compare our results with experimental data for Bi-doped Mg_2Si [58] and $Mg_2Si_{0.5}Ge_{0.5}$ [59] and virtual crystal approximation calculations for $Mg_2Si_{0.97}Sn_{0.03}$ alloys [13]. The values of the scattering parameter in these cases are 0.12, 0.19, and 0.25, correspondingly. As one can see in Fig. 8, perturbation theory in this regime shows overall good agreement with results of the previous investigations; however, it is clear that mass scattering alone slightly underestimates the reduction of thermal conductivity, as expected. It should also be noted that agreement for the largest scattering parameter is not very meaningful: the phonon mean free path in this regime is comparable with the interatomic distance; thus, the phonon-mediated thermal transport picture is breaking down. This is also evidenced in the fact that thermal conductivity is very weakly temperature dependent for scattering parameters greater than 0.5.

IV. CONCLUSIONS

In this paper, we have performed first-principles calculations of the thermal transport and anharmonic properties of the series of II-IV semiconductors, Mg_2X, X = C, Si, Ge, Sn, and Pb. The thermal conductivity of Mg_2C was calculated and predicted to be 34 W/mK at room temperature, a somewhat low value, considering the very low masses of its constituents. The thermal conductivities of the other compounds in the series agree well with the available experimental data and show a decreasing trend with increased mass. As a result of detailed analysis, this decrease was mainly attributed to the decrease of the phonon group velocity in the series, rather than any trend in the strength of anharmonicity. The contribution of the optical modes was also found to be significant, as previously seen in other fluorite compounds. We also found LDA to be more appropriate for the thermal transport calculations than GGA due to the slightly more accurate lattice constants, especially when thermal expansion is taken into account. Finally, our results for point defects scattering indicate that perturbation theory is reliable up to quite large values of the scattering parameter; however, inclusion of the force constant disorder might be necessary for accurate estimations of the effect. Our results also indicate that doping by heavy elements, such as Bi, in the amount of up to 1% will exhaust all the potential in reducing thermal conductivity by the point defect scattering.

ACKNOWLEDGMENTS

This paper was authored by subcontractors of the US Government under DOE Contract No. DE-AC07-05ID14517, under the Energy Frontier Research Center (Office of Science, Office of Basic Energy Science, FWP 1356). Accordingly, the U.S. Government retains and the publisher (by accepting the article for publication) acknowledges that the U.S. Government retains a nonexclusive, paid-up, irrevocable, worldwide license to publish or reproduce the published form of this manuscript, or allow others to do so, for US Government purposes.

[1] C. J. Buchenauer and M. Cardona, Raman scattering in Mg_2Si, Mg_2Ge, and Mg_2Sn, Phys. Rev. B **3**, 2504 (1971).

[2] J. J. Martin and H. R. Shanks, Thermal conductivity of magnesium plumbide, J. Appl. Phys. **45**, 2428 (1974).

[3] Y. Raptis, G. Kourouklis, E. Anastassakis, E. Haro-Poniatowski, and M. Balkanski, Anharmonic effects in Mg_2X (X = Si, Ge, Sn) compounds studied by Raman spectroscopy, J. Phys. France **48**, 239 (1987).

[4] G. H. Grosch and K.-J. Range, Studies on AB_2-type intermetallic compounds, I. Mg_2Ge and Mg_2Sn: single-crystal structure refinement and ab initio calculations, J. Alloys Compd. **235**, 250 (1996).

[5] P. Pandit and S. P. Sanyal, First principles study of electronic, elastic and lattice dynamical properties of Mg_2X (X = Si, Ge and Sn) compounds, Indian J. Pure Appl. Phys. **49**, 692 (2011).

[6] D. Zhou, J. Liu, S. Xu, and P. Peng, Thermal stability and elastic properties of Mg_2X (X = Si, Ge, Sn, Pb) phases from first-principle calculations, Comput. Mater. Sci. **51**, 409 (2012).

[7] O. O. Kurakevych, T. A. Strobel, D. Y. Kim, and G. D. Cody, Synthesis of Mg_2C: a magnesium methanide, Angew. Chem. Int. Ed. **52**, 8930 (2013).

[8] V. K. Zaitsev, M. I. Fedorov, E. A. Gurieva, I. S. Eremin, P. P. Konstantinov, A. Y. Samunin, and M. V. Vedernikov, Highly effective $Mg_2Si_{1-x}Sn_x$ thermoelectrics, Phys. Rev. B **74**, 045207 (2006).

[9] D. Tamura, R. Nagai, K. Sugimoto, H. Udono, I. Kikuma, H. Tajima, and I. J. Ohsugi, Melt growth and characterization of Mg_2Si bulk crystals, Thin Solid Films **515**, 8272 (2007).

[10] J. Tani and H. Kido, Lattice dynamics of Mg_2Si and Mg_2Ge compounds from first-principles calculations, Comput. Mater. Sci. **42**, 531 (2008).

[11] H. Wang, H. Jin, W. Chu, and Y. Guo, Thermodynamic properties of Mg_2Si and Mg_2Ge investigated by first principles method, J. Alloys Compd. **499**, 68 (2010).

[12] R. Viennois, P. Jund, C. Colinet, and J.-C. Tedenac, Defect and phase stability of solid solutions of Mg_2X with an antifluorite structure: an ab initio study, J. Solid State Chem. **193**, 133 (2012).

[13] W. Li, L. Lindsay, D. A. Broido, D. A. Stewart, and N. Mingo, Thermal conductivity of bulk and nanowire $Mg_2Si_xSn_{1-x}$ alloys from first principles, Phys. Rev. B **86**, 174307 (2012).

[14] L. Chaput, Direct Solution to the Linearized Phonon Boltzmann Equation, Phys. Rev. Lett. **110**, 265506 (2013).

[15] J. W. L. Pang, W. J. L. Buyers, A. Chernatynskiy, M. D. Lumsden, B. C. Larson, and S. R. Phillpot, Phonon Lifetime Investigation of Anharmonicity and Thermal Conductivity of UO_2 by Neutron Scattering and Theory, Phys. Rev. Lett. **110**, 157401 (2013).

[16] A. Chernatynskiy, J. E. Turney, A. J. H. McGaughey, C. H. Amon, and S. R. Phillpot, Phonon-mediated thermal conductivity in ionic solids by lattice dynamics-based methods, J. Am. Ceram. Soc. **94**, 3523 (2011).

[17] A. Ward, D. A. Broido, D. A. Stewart, and G. Deinzer, *Ab initio* theory of the lattice thermal conductivity in diamond, Phys. Rev. B **80**, 125203 (2009).

[18] X. Tang and J. Dong, Lattice thermal conductivity of MgO at conditions of Earth's interior, Proc. Natl. Acad. Sci. USA **107**, 4539 (2010).

[19] Z. Tian, J. Garg, K. Esfarjani, T. Shiga, J. Shiomi, and G. Chen, Phonon conduction in PbSe, PbTe, and $PbTe_{1-x}Se_x$ from first-principles calculations, Phys. Rev. B **85**, 184303 (2012).

[20] A. Chernatynskiy and S. R. Phillpot, Thermal conductivity of argon at high pressure from first principles calculations, J. Appl. Phys. **114**, 064902 (2013).

[21] L. Lindsay, D. A. Broido, and T. L. Reinecke, *Ab initio* thermal transport in compound semiconductors, Phys. Rev. B **87**, 165201 (2013).

[22] A. Chernatynskiy and S. R. Phillpot, Phonon transport simulator (PhonTS), Comp. Phys. Comm. **192**, 196 (2014).

[23] A. Chernatynskiy and S. R. Phillpot, Evaluation of computational techniques for solving the Boltzmann transport equation for lattice thermal conductivity calculations, Phys. Rev. B **82**, 134301 (2010).

[24] P. G. Klemens, in *Thermal Conductivity and Lattice Vibrational Modes*, Solid State Physics Vol. 7, edited by F. Seitz and D. Turnbull (Academic Press, New York, 1958), p. 1.

[25] B. Fultz, Vibrational thermodynamics of materials, Prog. Mater. Sci. **55**, 247 (2010).

[26] S. Baroni, P. Giannozzi, and E. Isaev, Density-functional perturbation theory for quasi-harmonic calculations, Rev. Mineral. Geochem. **71**, 39 (2010).

[27] G. Kresse and J. Hafner, *Ab initio* molecular dynamics for liquid metals, Phys. Rev. B **47**, 558 (1993).

[28] G. Kresse and J. Hafner, *Ab initio* molecular-dynamics simulation of the liquid-metal/amorphous-semiconductor transition in germanium, Phys. Rev. B **49**, 14251 (1994).

[29] G. Kresse and J. Furthmüller, Efficient iterative schemes for *ab initio* total-energy calculations using a plane-wave basis set, Phys. Rev. B **54**, 11169 (1996).

[30] G. Kresse and J. Furthmüller, Efficiency of *ab initio* total energy calculations for metals and semiconductors using a plane-wave basis set, Comp. Mater. Sci. **6**, 15 (1996).

[31] G. Kresse and D. Joubert, From ultrasoft pseudopotentials to the projector augmented-wave method, Phys. Rev. B **59**, 1758 (1999).

[32] P. E. Blöchl, Projector augmented-wave method, Phys. Rev. B **50**, 17953 (1994).

[33] A. Konti and Y. P. Varshni, Debye temperatures of 24 cubic elements by three methods, Can. J. Phys. **47**, 2021 (1969).

[34] R. Schwartz, H. Shanks, and B. Gerstein, Thermal study of II-IV semiconductors: heat capacity and thermodynamic functions of Mg_2Pb from 5–300 K, J. Solid State Chem. **3**, 533 (1971).

[35] J. Hao, B. Zou, P. Zhu, C. Gao, Y. Li, D. Liu, K. Wang, W. Lei, Q. Cui, and G. Zou, *In situ* x-ray observation of phase transitions in under high pressure, Solid State Commun. **149**, 689 (2009).

[36] C. R. Whitsett and G. Danielson, Electrical properties of magnesium silicide and magnesium germanide, Technical Report, Ames Laboratory, Iowa State College, 1955.

[37] B. Gerstein, P. Chung, and G. Danielson, Thermal study of group II-IV semiconductors-I. heat capacity of Mg_2Ge in the range 5–300 K, J. Phys. Chem. Solids **27**, 1161 (1966).

[38] B. C. Gerstein, F. J. Jelinek, M. Habenschuss, W. D. Shickell, J. R. Mullaly, and P. L. Chung, Thermal study of groups II-IV semiconductors. Lattice heat capacities and free energies of formation. Heat capacity of Mg_2Si from 15–300 K, J. Chem. Phys. **47**, 2109 (1967).

[39] D. Bessas, R. E. Simon, K. Friese, M. Koza, and R. P. Hermann, Lattice dynamics in intermetallic Mg_2Ge and Mg_2Si, J. Phys.: Condens. Matter **26**, 485401 (2014).

[40] I. Dutchak and V. Yarmolyuk, X-ray characteristic temperature and thermal expansion coefficient of Mg_2Ge, Sov. Phys. J. **16**, 1606 (1973).

[41] P. Chung, W. Whitten, and G. Danielson, Lattice dynamics of Mg_2Ge, J. Phys. Chem. Solids **26**, 1753 (1965).

[42] L. Davis, W. Whitten, and G. Danielson, Elastic constants and calculated lattice vibration frequencies of Mg_2Sn, J. Phys. Chem. Solids **28**, 439 (1967).

[43] G. A. Slack, in *The Thermal Conductivity of Non-Metallic Solids*, Solid State Physics Vol. 34, edited by H. Ehrenreich, F. Seitz, and D. Turnbull (Academic Press, New York, 1973), p. 1.

[44] D. Pollock, *Physical Properties of Materials for Engineers* (Taylor & Francis, Boca Raton, 1993).

[45] H. Ishii, S. Matsuo, P. Karimov, K. Tanaka, and J. Kawai, Effective charge on silicon atom in the metal silicides Mg_2Si and CaSi, Phys. Rev. B **71**, 205202 (2005).

[46] M. R. J. van Buuren, F. Voermans, and H. vanKempen, Bonding in Mg_2Si studied with x-ray photoelectron spectroscopy, J. Phys. Chem. **99**, 9519 (1995).

[47] D. McWilliams and D. W. Lynch, Infrared reflectivities of magnesium silicide, germanide, and stannide, Phys. Rev. **130**, 2248 (1963).

[48] A. Kato, T. Yagi, and N. Fukusako, First-principles studies of intrinsic point defects in magnesium silicide, J. Phys.: Condens. Matter **21**, 205801 (2009).

[49] L. Chuang, N. Savvides, and S. Li, Magnetron deposition of in situ thermoelectric Mg_2Ge thin films, J. Electron. Mater. **38**, 1008 (2009).

[50] M. Hutchings, T. Farley, M. Hackett, W. Hayes, S. Hull, and U. Steigenberger, Neutron scattering investigation of lattice dynamics and thermally induced disorder in the antifluorite Mg_2Si, Solid State Ionics **28**, 1208 (1988).

[51] R. Kearney, T. Worlton, and R. Schmunk, Lattice dynamics of magnesium stannide at room temperature, J. Phys. Chem. Solids **31**, 1085 (1970).

[52] N. Wakabayashi, A. A. Z. Ahmad, H. R. Shanks, and G. C. Danielson, Lattice dynamics of Mg_2Pb at room temperature, Phys. Rev. B **5**, 2103 (1972).

[53] T. Li, W. Ju, H. Liu, H. Cui, X. Zhao, Y. Yong, and Z. Feng, First-principles investigation of the electronic and lattice vibrational properties of Mg_2C, Comput. Mater. Sci. **93**, 234 (2014).

[54] L. Chaput, J. Bourgeois, A. Prytuliak, M. M. Koza, and H. Scherrer, Simple view of the $Mg_2Si_{1-x}Sn_x$ phonon spectrum: Sn resonances and mean field, Phys. Rev. B **91**, 064304 (2015).

[55] G. Leibfried and E. Schlomann, Wärmeleitung in elektrisch isolierenden Kristallen, Nachr. Akad. Wiss. Goett. Math.-Phys. Kl. **4**, 71 (1954).

[56] C. F. Gallo, R. C. Miller, P. H. Sutter, and R. W. Ure, Bipolar electronic thermal conductivity in semimetals, J. Appl. Phys. **33**, 3144 (1962).

[57] S.-i. Tamura, Isotope scattering of large-wave-vector phonons in GaAs and InSb: Deformation-dipole and overlap-shell models, Phys. Rev. B **30**, 849 (1984).

[58] S. K. Bux, M. T. Yeung, E. S. Toberer, G. J. Snyder, R. B. Kaner, and J.-P. Fleurial, Mechanochemical synthesis and thermoelectric properties of high quality magnesium silicide, J. Mater. Chem. **21**, 12259 (2011).

[59] X. Zhou, G. Wang, H. Chi, X. Su, J. Salvador, W. Liu, X. Tang, and C. Uher, Thermoelectric performance of Sb- and La-doped $Mg_2Si_{0.5}Ge_{0.5}$, J. Electron. Mater. **41**, 1589 (2012).